Autonomous Flexible Endoscope for Minimally Invasive Surgery With Enhanced Safety

Xin Ma, Chengzhi Song, Philip Waiyan Chiu, and Zheng Li, *Member, IEEE*

***Abstract*—Automation in robotic surgery has become an increasingly attractive topic. Although full automation remains fictional, task autonomy and conditional autonomy are highly achievable. Apart from the performance of task fulfillment, one major concern in robotic surgery is safety. In this paper, we present a flexible endoscope that can help to guide the minimally invasive surgical operations automatically. It is developed based on the tendon-driven continuum mechanism and is integrated with the da Vinci research kit. In total, the proposed flexible endoscope has six degree-of-freedoms. Visual servoing is adopted to automatically track the surgical instruments. During the tracking, optimal control method is used to minimize the motion and space occupation of the flexible endoscope, which will improve the safety of both the robot system and the assistants nearby. Compared with the existing rigid endoscope, both the experimental results and the user study results show that the proposed flexible endoscope has advantages of being safer and less space occupation without reducing its comfort level.**

***Index Terms*—Surgical robotics, laparoscopy, visual tracking, robot safety.**

I. Introduction

MINIMALLY invasive surgery (MIS) is becoming a standard of care due to its advantages over open surgery such as less blood loss, shorter hospital stay, less postoperative pain and better cosmesis [1]. In MIS, an endoscope is inserted into the patient's body to guide surgical operations. Typically, the endoscope is held and maneuvered by an assistant, namely an endoscope holder, during the surgery. The assistant maneuvers the endoscope to view the region of interest (ROI) and places the ROI in the center of the endoscope view [2]. Yet, holding the endoscope is physically demanding. In lengthy surgeries, endoscope holder would suffer from fatigue, which may, in turn, affect the performance. One promising approach of addressing the problem is to develop automatic endoscopes that can adjust the view without frequent instructions from surgeons. Apart from providing the desired view, another important consideration is safety. For example, during surgeries, it has to be made sure that the endoscope does not collide with the surgical instruments inside the body cavity and the clinician/instruments outside the body cavity.

To reduce the fatigue of assistant surgeons, the endoscope holder could be robotized and controlled by surgeons [4]. For example, Naviot [5] proposed a remotely operated endoscope which can be manipulated with buttons. However, surgeons cannot reach the buttons when both hands are occupied. In the da Vinci Surgical System (Intuitive Surgical Inc., Sunnyvale, CA) and AESOP (Automated Endoscopic System for Optimal Positioning) system [6], the surgeon controls the endoscopic manipulator by switching the control mode. Nonetheless, the motion of the endoscope and instruments cannot be controlled at the same time [7]. Kim *et al.* proposed an improved novel master interface (iNMS) based endoscope control method and system. However, the iNMS is controlled by the hands of the surgeon who operates the da Vinci Surgical System, which increases the difficulty of the surgery [8].

An alternate way is to control the view of the endoscope by using the facial/eye/mouth motion or the voice of the operating surgeon. Firstly, a novel human–machine interface that can track surgeons' facial motions has been proposed to control the view of the endoscope [9]. However, it is difficult for surgeons to control their facial motions during surgeries. Then, a voice-controlled robotic assisting scope holder AESOP is developed [10]. However, voice based control methods prevent surgeons from giving verbal orders to assistants, which is essential during surgical operations. Eye-motion based method is another popular hands-off endoscope control method. Eye movements are essential motor movements controlled by human cognitive system [11], [12]. Stand-alone eye trackers are used to obtain the position of the eye gaze to control endoscope. However, the effects of unconscious eye movements (glancing and saccades) pose great challenges for eye tracking based endoscope control system.

Another popular hands-off endoscope control method is tip tracking based method. A novel tip tracking control method for a rigid robotic endoscope holder during laparoscopic surgeries is proposed and applied to the robot ViKY [15]. With this method, additional sensors and attention of operating surgeons are not needed to control the view of the endoscope. There is no doubt that these systems/methods could help surgeons to control the endoscope. However, the safety factors are not adequately taken into consideration in these automatic endoscope systems. These

Manuscript received September 8, 2018; accepted January 8, 2019. Date of publication January 28, 2019; date of current version April 30, 2019. This letter was recommended for publication by Associate Editor P. R. Culmer and Editor P. Valdastri upon evaluation of the reviewers' comments. This work was supported in part by the Hong Kong General Research Grant with Project 14212316, in part by Early Career Scheme with Project 24204818, and in part by the SJTU-CUHK Project. *(Corresponding author: Zheng LI.)*

X. Ma is with the Chow Yuk Ho Technology Centre for Innovative Medicine, Chinese University of Hong Kong, Hong Kong (e-mail: Maxin2000@mail.dlut.edu.cn).

C. Song, P. W. Chiu, and Z. LI are with the Department of Surgery and the Chow Yuk Ho Technology Centre for Innovative Medicine, Chinese University of Hong Kong, Hong Kong (e-mail: songchengzhiinhk@gmail.com; philipchiu@surgery.cuhk.edu.hk; lizheng@cuhk.edu.hk).

Digital Object Identifier 10.1109/LRA.2019.2895273

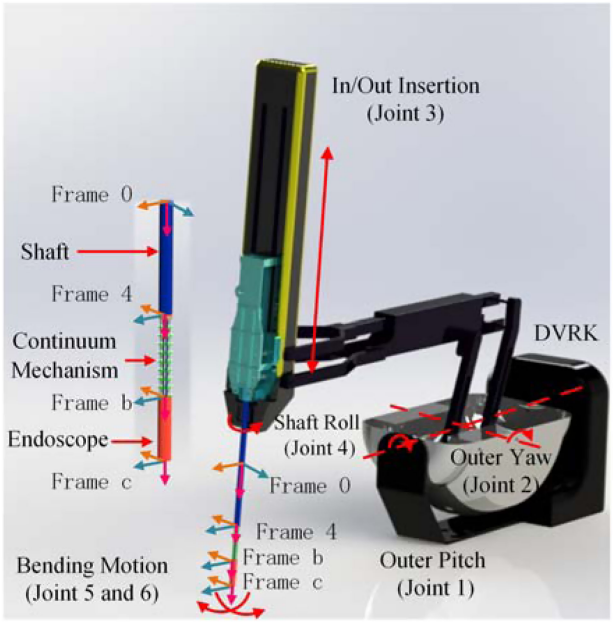

Fig. 1. The structure of the 6-DOF flexible endoscope. The proposed flexible endoscope has six DOFs, where joint 1, 2, 3, 4 of the PSM control the pitch, yaw, insertion and roll of the proposed flexible endoscope, respectively; joint 5 and 6 of the PSM control the bending of the TCM.

systems are built on commercial rigid endoscopes which rely on pivoting motion to adjust the viewing direction.

In this work, a 6-DOF automatic flexible endoscope integrated with the DVRK is proposed, as shown in Fig. 1. The proposed flexible endoscope could adjust its view by tracking surgical instruments, which frees the hands of surgeons. More importantly, combined with the optimal control, both the internal space and the external space occupied by the flexible endoscope during the operation is minimized. This could avoid potential instruments fencing and improve the safety of surgeries. The main contribution of this paper is as follows:

1) developed a 6-DOF automatic flexible endoscope based on the tendon-driven continuum mechanism (TCM) and integrated it with the DVRK;
2) developed the kinematic model of the 6-DOF automatic flexible endoscope and achieved instruments tracking with visual servoing control;
3) developed the optimal control of the 6-DOF flexible endoscope with minimal motion, and studied the space occupation of rigid endoscope and flexible endoscope during instruments tracking process.

The rest of this paper is organized as follows. In Section II, the kinematic model of the 6-DOF flexible endoscope is introduced. In Section III, the vision-based tacking method and model are elaborated. In Section IV, the optimal control method for the 6-DOF flexible endoscope is proposed. In Section V, the experimental results are shown in detail. At last, Section VI concludes this work.

II. Flexible Endoscope

As shown in Fig. 1, the proposed flexible endoscope has six DOFs, where joint 1, 2, 3, 4 of the PSM control the pitch, yaw, insertion and roll of the flexible endoscope; joint 5 and 6 of the PSM control the bending of the TCM. The TCM could bend in two orthogonal directions independently [19], [20]. And it is connected to a rigid shaft, which can roll and translate. Therefore, the first four joints of the proposed flexible endoscope are conventional rigid joints (rigid part) and the last two joints of the proposed flexible endoscope control the TCM (flexible part). In the following parts, the kinematics model of the 6-DOF flexible endoscope is introduced.

A. The Kinematics of Rigid Part

TCM is installed on the 4th frame of the PSM (origin of frame $\{4\}$), so the transformation from space frame (frame $\{0\}$) to frame $\{4\}$ of the proposed flexible endoscope is the same as the transformation from space frame (frame $\{0\}$) to frame $\{4\}$ of the PSM, as shown in Fig. 1. The forward kinematics of the rigid part can be computed by using Denavit–Hartenberg (D-H) convention:

$$^{0}\boldsymbol{T}_{4} = {}^{0}\boldsymbol{T}_{1}{}^{1}\boldsymbol{T}_{2}{}^{2}\boldsymbol{T}_{4}{}^{3}\boldsymbol{T}_{4} \tag{1}$$

where ${}^{i}\boldsymbol{T}_{j}$ represents the transformation from frame $\{\mathrm{i}\}$ to frame $\{\mathrm{j}\}$; ${}^{3}\boldsymbol{T}_{4}$, ${}^{2}\boldsymbol{T}_{3}$, ${}^{1}\boldsymbol{T}_{2}$, ${}^{0}\boldsymbol{T}_{1}$ are the homogeneous transformation matrixes of the 4th 3rd 2nd and 1st joint respectively, which can be found in reference [16]. The velocity of each joints of the rigid part ($\dot{\boldsymbol{Q}}_{rigid}$) is related to direct kinematics via a Jacobian matrix $\boldsymbol{J}_{rigid}$ for rigid part shown below:

$$^{0}\dot{\boldsymbol{X}}_{4} = \boldsymbol{J}_{rigid}\dot{\boldsymbol{Q}}_{rigid} \tag{2}$$

where ${}^{0}\dot{\boldsymbol{X}}_{4}$ is the velocity vector which consists of linear velocity and angular velocity for the frame $\{4\}$ represented in space frame $\{0\}$.

B. The Kinematics of Flexible Part

The TCM is installed on the 4th frame of the PSM. Therefore, frame $\{4\}$ is the base frame of the flexible part of the proposed endoscope. The homogeneous transformation matrix from frame $\{4\}$ to the body frame (${}^{4}\boldsymbol{T}_{b}$) of the TCM can be calculated [17], [18] as in equation (3) shown at the bottom of this page, where θ is the bending angle of the flexible part; Φ is the bending direction of the TCM and l is the length of the flexible part. The linear and angular velocity related to flexible

$$^{4}\boldsymbol{T}_{b} = \begin{bmatrix} \cos^{2}\Phi(\cos\theta-1)+1 & \sin\Phi\cos\Phi(\cos\theta-1) & \cos\Phi\sin\theta & \frac{l}{\theta}(1-\cos(\theta))\cos(\Phi) \\ \sin\Phi\cos\Phi(\cos\theta-1) & \cos^{2}\Phi(1-\cos\theta)+\cos\theta & \sin\Phi\sin\theta & \frac{l}{\theta}(1-\cos(\theta))\sin(\Phi) \\ -\cos\Phi\sin\theta & -\sin\Phi\sin\theta & \cos\theta & \frac{l}{\theta}\sin(\theta) \\ 0 & 0 & 0 & 1 \end{bmatrix} \tag{3}$$

part can be drawn from the below Jacobian matrix ($\boldsymbol{J}_{flex}$):

$$\boldsymbol{J}_{flex} = \begin{bmatrix} \sin\Phi(\cos\theta - 1)\frac{l}{\theta} & \frac{l}{\theta^2}\cos\Phi(\cos\theta + \theta\sin\theta - 1) \\ -\cos\Phi(\cos\theta - 1)\frac{l}{\theta} & \frac{l}{\theta^2}\sin\Phi(\cos\theta + \theta\sin\theta - 1) \\ 0 & -\frac{l}{\theta^2}(\sin\theta - \theta\cos\theta) \\ -\cos\Phi\sin\theta & -\sin\Phi \\ -\sin\Phi\sin\theta & \cos\Phi \\ 1 - \cos\theta & 0 \end{bmatrix} \tag{4}$$

The velocity of the joints of the flexible part is shown as:

$$^4\dot{\boldsymbol{X}}_b = \boldsymbol{J}_{flex}\dot{\boldsymbol{Q}}_{flex} \tag{5}$$

in which $\dot{\boldsymbol{Q}}_{flex}$ is the velocity of the joints with respect to the flexible part. $^4\dot{\boldsymbol{X}}_b$ is the vector consisting of the linear velocity and angular velocity for the body frame {b} of the TCM represented in frame {4}.

C. The Kinematics of the 6-DOF Flexible Endoscope

The forward kinematics model of the 6-DOF flexible endoscope is shown below:

$$^0\boldsymbol{T}_c = {}^0\boldsymbol{T}_4\,{}^4\boldsymbol{T}_b\,{}^b\boldsymbol{T}_c = {}^0\boldsymbol{T}_4\,{}^4\boldsymbol{T}_c \tag{6}$$

where

$$^b\boldsymbol{T}_c = \begin{bmatrix} 1 & 0 & 0 & 0 \\ 0 & 1 & 0 & 0 \\ 0 & 0 & 1 & l_{bc} \\ 0 & 0 & 0 & 0 \end{bmatrix}$$

is a constant link transformation matrix from body frame {b} of TCM to camera frame {c}. l_{bc} is the distance between the origin of the body frame {b} and optical center of the endoscope. The velocity of end-effector of the 6-DOF flexible endoscope can be computed by:

$$\dot{\boldsymbol{X}} = \boldsymbol{J}\dot{\boldsymbol{Q}} \tag{7}$$

where $\dot{\boldsymbol{Q}}$ is the velocity of each joints of the 6-DOF flexible endoscope. The velocity map of 6-DOF flexible endoscope (J) is given by following 6×6 Jacobian matrix:

$$\boldsymbol{J} = \begin{bmatrix} \boldsymbol{J}_{rigid} & \boldsymbol{J}_{flex} \end{bmatrix} \tag{8}$$

III. Vision Feedback

This section first presents the surgical instruments tracking method of the proposed flexible endoscope, and then introduces the visual servoing model.

A. Tracking Method

To automatically track the motion of surgical instruments with the proposed 6-DOF flexible endoscope, the coordinates of the markers on the images need to be obtained [19]. Difficulties for tracking the surgical instruments are as follows: (1) the rapid changing of the background of the images obtained by endoscope; (2) the instruments' rolling motion and the uncertainty of the number of instruments.

In this paper, green is chosen as the marker's color, since it is rarely seen naturally inside human bodies. Markers are applied to the surface of the surgical instruments' distal end. The tracking method is as follows: (1) At first, green areas on each RGB frame are recognized on the basis of the color-based image segmentation method [21]. Once green area detection is complete, the RGB frame is converted to gray scale where it is then smoothed by using a Gaussian filter. (2) Then image connected regions are selected and the connected areas below a fixed size threshold (60 pixels) are removed. The threshold selected is based on the size of the original RGB image so that a range of cameras are applicable. (3) Lastly, the gray centroid method is used to obtain the center coordinates of all selected connected areas. And the mean value of these center coordinates is used as tracking points to control the motion of the proposed 6-DOF flexible endoscope as shown in Fig. 2.

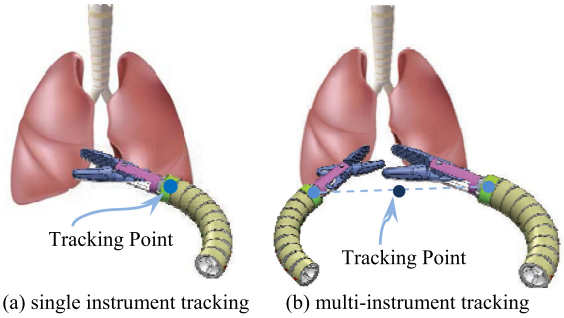

Fig. 2. The principle of vision tracking. The green markers are attached on the tip of the surgical instruments.

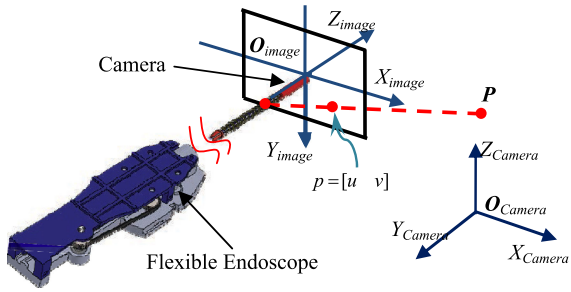

Fig. 3. The principle of pinhole model. $\boldsymbol{P}$ is the positional coordinate in the camera coordinate system. p is the positional coordinate in the image coordinate system.

B. Visual Servo Model

Camera model is the relationship between the 2D information of images and the 3D information of the world. In the following part, two types of coordinate systems (image and global coordinate systems) are involved in transforming the 2D image coordinates obtained from the camera to 3D global coordinates information, as shown in Fig. 3.

In this paper, pinhole model is taken as the imaging model, which can be written as the following equation [20], [22]:

$$Z_c \begin{bmatrix} u \\ v \\ 1 \end{bmatrix} = \begin{bmatrix} f/\rho_w & 0 & u_0 & 0 \\ 0 & f/\rho_h & v_0 & 0 \\ 0 & 0 & 1 & 0 \end{bmatrix} \begin{bmatrix} x \\ y \\ z \\ 1 \end{bmatrix} \tag{9}$$

where $(u_0\ v_0)$ represents the center coordinate of image captured by the endoscope; $(u\ v)$ represents the extracted image

coordinate after image distortion correcting; $P = [x, y, z]^T$ is the positional coordinate in the camera coordinate system; Z_c is the scale factor; f is the focal length of the lens; ρ_w and ρ_h are the weight and length of each pixel on the image sensor. In typical cases where $\rho_w = \rho_h$, we can express the focal length in pixels $\lambda = f/\rho_w = f/\rho_h$; The distortion of the endoscope is corrected by using the method in reference [20]. Then we use a state-of-the-art 2D visual servoing control approach (image-based control) to control the motion of the proposed flexible endoscope. $[\dot{u}\ \dot{v}]$ can be obtained by [23]:

$$\begin{bmatrix}\dot{u}\\ \dot{v}\end{bmatrix} = \begin{bmatrix}\frac{\lambda}{z} & 0 & -\frac{u}{z} & -\frac{uv}{\lambda} & \frac{\lambda^2+u^2}{\lambda} & -v\\ 0 & \frac{\lambda}{z} & -\frac{v}{z} & \frac{-\lambda^2-v^2}{\lambda} & \frac{uv}{\lambda} & -u\end{bmatrix}\begin{bmatrix}v_x\\ v_y\\ v_z\\ \omega_x\\ \omega_y\\ \omega_z\end{bmatrix}$$
$$= \left[\frac{1}{z}\boldsymbol{H}_V, \boldsymbol{H}_\omega\right]\cdot\dot{\boldsymbol{X}} = \left[\frac{1}{z}\boldsymbol{H}_V, \boldsymbol{H}_\omega\right]\cdot\boldsymbol{J}\cdot\dot{\boldsymbol{Q}} \quad (10)$$

Suppose that the end-effector is moving with both angular velocity $[\omega_x\ \omega_y\ \omega_z]$ and translation velocity $[v_x\ v_y\ v_z]$ with respect to the camera frame in fixed camera system. $\boldsymbol{H}_\omega = \begin{bmatrix}-uv/\lambda & (\lambda^2+u^2)/\lambda & -v\\ (-\lambda^2-v^2)/\lambda & uv/\lambda & -u\end{bmatrix}$, $\boldsymbol{H}_V = \begin{bmatrix}\lambda & 0 & -u\\ 0 & \lambda & -v\end{bmatrix}$. We can see that the parameter z in Jacobian is also unknown. Therefore, we use the measurements of robot and image motion to online estimate the value of z. The value of z can be linearly estimated from equation (10) by using least-squares [24].

IV. Vision-Based Control Method

In this part, an optimal control with constraints of minimal motion is proposed firstly. Then visual servoing control loop for 6-DOF flexible endoscope is introduced.

A. Optimal Control With Minimal Movement

In the optimal control algorithm, a penalty function to optimize $\boldsymbol{Q}^k = (q_1^k, q_2^k, q_3^k, q_4^k, q_5^k, q_6^k)$ is employed [25]. q_i^j is the movement of the $i-th$ joint at the time j. The constraints for the boundary minimum are:

$$q_1^k < q_1^{\max} \text{ and } q_2^k < q_2^{\max} \quad (11)$$

With constraints (11), the following penalty function is developed as:

$$f(\boldsymbol{Q}^k) = \alpha\left(\left\|q_1^k - q_1^{k-1}\right\| + \left\|q_2^k - q_2^{k-1}\right\|\right) + \beta\left(\left\|q_3^k - q_3^{k-1}\right\| + \left\|q_4^k - q_4^{k-1}\right\| + \left\|q_5^k - q_5^{k-1}\right\| + \left\|q_6^k - q_6^{k-1}\right\|\right) + r_1\min\left\{0, q_1^{\max} - q_1^k\right\}^2 + r_2\min\left\{0, q_2^{\max} - q_2^k\right\}^2 \quad (12)$$

where r_1 and r_2 are safety factors which make sure that the value of q_1^k is smaller than $q_1^{\max}$ and the value of q_2^k is smaller than$q_2^{\max}$. The factor α and β are weight factors to reduce the movements of the first and the second joint. And the parameters $q_1^k, q_2^k, q_3^k, q_4^k, q_5^k$ and q_6^k can be estimated by minimizing the objective function equation (13). Here the Levenberg–Marquardt algorithm is used to perform the optimization.

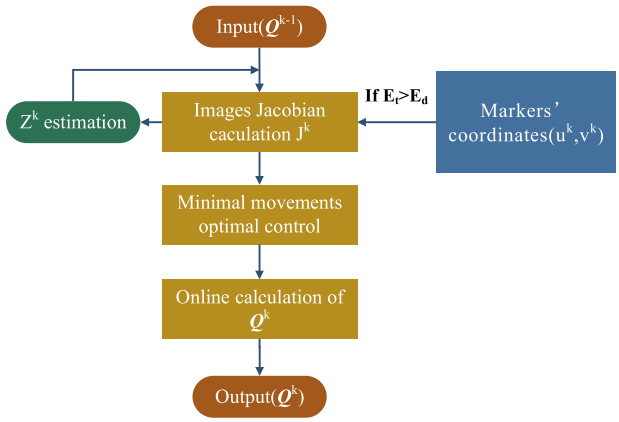

Fig. 4. Framework of the control loop for tracking the tips. After target's depth information estimating, the images jacobian can be calculated. Then the proposed minimal movements optimal control method is used to online obtain the value of the $\boldsymbol{Q}^k$.

$$\begin{aligned}&\text{minimize} \quad f(\boldsymbol{Q}^k)\\ &\text{subject to} \quad \begin{bmatrix}\dot{u}\\ \dot{v}\end{bmatrix} = \left[\frac{1}{z}\boldsymbol{H}_V, \boldsymbol{H}_\omega\right]\cdot\boldsymbol{J}\cdot\dot{\boldsymbol{Q}}\end{aligned} \quad (13)$$

B. Control Loop for Tracking the Instruments

The developed flexible endoscope is installed onto the PSM and controlled by computer. Fig. 4 shows the overall framework of the visual servoing control method.

As shown in Fig. 4, in the tracking framework, the image coordinate (u^k, v^k) of targets is obtained by the endoscope. Then the tracking error E_t can be calculated by:

$$E_t = \sqrt{(u^k - u_d)^2 + (v^k - v_d)^2} \quad (14)$$

where (u_d, v_d) is the desired image coordinate of the target and E_d is the permissible error. If $E_t > E_d$, the image Jacobian $(\boldsymbol{J}^k)$ and the depth information of the target (Z^k) can be estimated via equation (10). Then by using the proposed optimal control method, the motion of each joint $(\boldsymbol{Q}^k)$ can be minimized. Lastly, controllers will give command to the actuators and make sure the flexible endoscope can reach the desired position and orientation.

V. Experiments

In this section, tracking performances of stationary and moving targets are tested at first. Then, ex vivo experiments and surgical FLS tasks are done to evaluate the performance of the proposed 6-DOF flexible endoscope. Lastly, user experiences are studied to compare the proposed flexible endoscope with rigid endoscope.

A. Experimental Setup

As shown in Fig. 5, the test setup includes two parts: a 6-DOF flexible endoscope and a DVRK. The PSM is controlled by the DVRK controller. The flexible endoscope includes 3

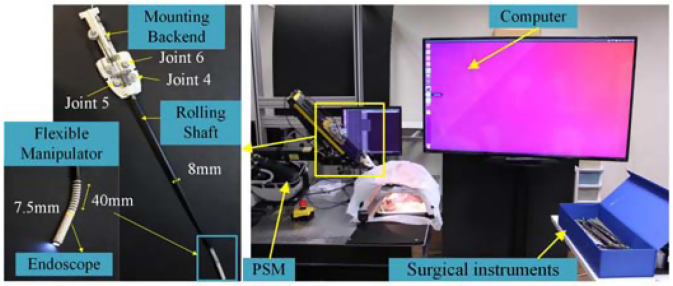

Fig. 5. The experimental platform. The test bench includes two parts: a 6-DOF flexible endoscope and a PSM of the DVRK. A computer is used to display the images obtained from the endoscope. A number of surgical instruments with green markers are prepared for ex vivo experiments.

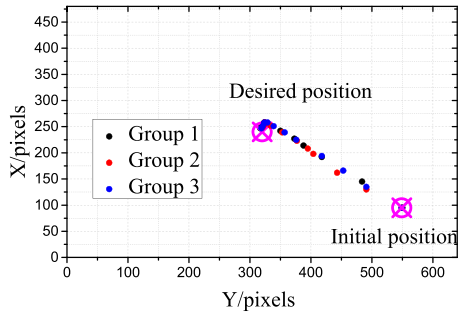

Fig. 6. Target tracking trajectory on the image. The pink symbols are the desired position and initial position of the target on the image. The color points are the coordinates of the target in each step during tracking.

TABLE I
ENDOSCOPE PARAMETERS

u_0	v_0	λ	r_1	r_2	k_1	k_2
319.2 pixels	243.8 pixels	810.2	0.0088	-0.17	0.0006	0.0012

components: (1) a camera with the resolution of 640 × 480 pixels is installed on the distal end, communicating with computer through USB. Its frame rate can reach 30 Hz; (2) flexible bending section consisting of 10 vertebras with an elastic backbone. The length of the flexible bending section is 40 mm and the outer diameter is 7.5 mm; (3) a rolling shaft from the DVRK instruments and self-designed mounting back-end.

The endoscope has been calibrated with Zhang's calibration method [20]. And the endoscope parameters are shown in Table I. k_1, k_2, p_1 and p_2 stand for the first order radial distortion coefficient, the second order radial distortion coefficient, the first order tangential distortion coefficient and the second order tangential distortion coefficient respectively.

B. Tracking Stationary Target

In this part, a stationary green marker is tracked three times by the 6-DOF flexible endoscope system. The diameter of the marker is 3 mm. The value of the permissible error is set as 10 pixels ($E_d = 10$ pixels). The target image coordinate (u_d, v_d) is the center coordinate of the image (320, 240) and the initial position is at the lower right corner. The tests are repeated three times and the tracking trajectories are shown in Figure 6. Results show that the tracking is reliable.

The tracking error (E_t) in each convergence step is shown in Fig. 7(a). The color points show that the value of the tracking error E_t reduces to 10 pixels in 11 steps. At the first 4 steps, the value of tracking error E_t is decreasing rapidly from 270 pixels to less than 100 pixels.

The tracking time in each convergence step is shown in Fig. 7(b). The tracking error E_t will drop from 270 pixels to 10 pixels within 1.71 seconds. And the tracking speed is mainly determined by the movement distance of the proposed flexible endoscope.

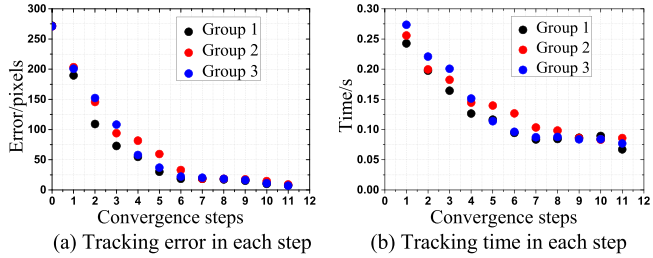

(a) Tracking error in each step (b) Tracking time in each step

Fig. 7. (a) Color points shows the value of the tracking error E_t reduces to 10 pixels in 11 convergence steps. (b) The color points are the tracking time in each convergence step during tracking processing.

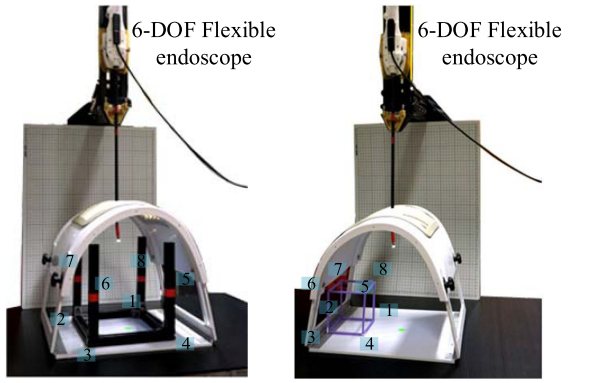

(a) tracking in rectangular space (200*mm* 200*mm*×100*mm*) (b) tracking in cube space (100*mm*×100*mm*×100*mm*)

Fig. 8. Moving target tracking experiment. A surgical instrument attached by a green marker is used as a moving target. The instrument passes through the 1st, 2nd, 3rd, 4th, 5th, 6th, 7th, 8th point. The 4-DOF rigid endoscope and the 6-DOF flexible endoscope are used to track the surgical instrument.

C. Tracking Moving Targets

In this part, the tracking performance of the proposed 6-DOF flexible endoscope is tested to compare with that of a 4-DOF endoscope. The 4-DOF rigid endoscope has the same viewing angle and the same resolution as the proposed flexible endoscope. Then the proposed 6-DOF flexible endoscope and the 4-DOF endoscope are used to track a moving target in two different spaces (200 mm × 200 mm × 100 mm rectangular space and 100 mm × 100 mm × 100 mm cube space). The moving trajectory is shown in Fig. 8 (the target passes through the 1st, 2nd, 3rd, 4th, 5th, 6th, 7th, 8th point in sequence).

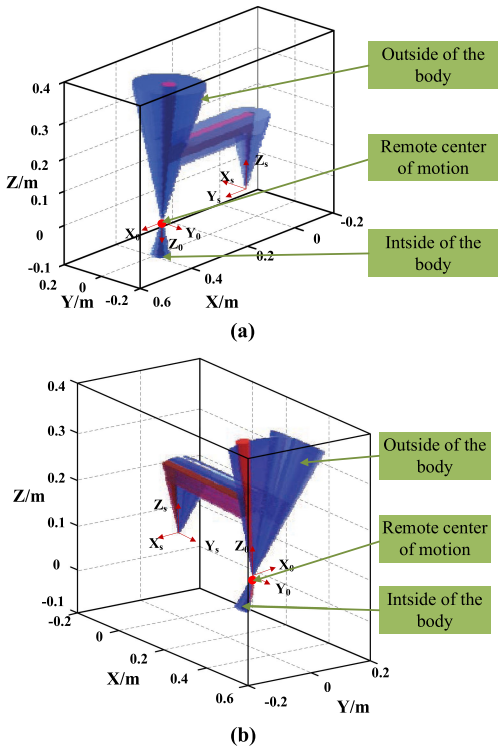

Fig. 9. Comparison of spaces occupied by the 4-DOF rigid endoscope (in blue) and the 6-DOF flexible endoscope (in red). (a) tracking a rectangular space with a dimension of 200 mm × 200 mm × 100 mm; (b) tracking a cubic space with a dimension of 100 mm × 100 mm × 100 mm.

As shown in Fig. 9(a), the blue area is the motion space of the 4-DOF endoscope in the process of tracking the moving target in the rectangular space. The red area is the motion space of the 6-DOF flexible endoscope in the process of tracking the moving target in the same space. The motion space of the 6-DOF flexible endoscope is 8.05 cm^3 inside the body and 580.16 cm^3 outside the body. By contrast, the motion space of the 4-DOF endoscope is 51.44 cm^3 inside the body and 5903.1 cm^3 outside the body. The motion space of the 6-DOF flexible endoscope is reduced to 15.55% of the motion space of the 4-DOF rigid endoscope inside the body and 9.83% of the motion space of the 4-DOF rigid endoscope outside the body.

And as shown in Fig. 9(b), the blue area is the motion space of the 4-DOF endoscope which tracks a moving target in cube space, and the red area is the motion space of the 6-DOF flexible endoscope which tracks a moving target in the same space. The motion space of the 6-DOF flexible endoscope is 2.87 cm^3 inside the body and 301.64 cm^3 outside the body. And the motion space of the 4-DOF endoscope is 11.56 cm^3 inside the body and 1882.3 cm^3 outside the body. The motion space of the proposed 6-DOF flexible endoscope is reduced to 24.83% of the motion space of the 4-DOF rigid endoscope inside the body and 16.3% of the motion space of the 4-DOF rigid endoscope outside the body.

D. Ex Vivo Experiments

In this section, ex vivo tests are conducted to evaluate the feasibility of the proposed 6-DOF flexible endoscope. As shown in Fig. 10, porcine stomach and intestine are placed in a position that resembles the one in vivo. The flexible endoscope is used to guide a surgical instrument to inspect the overall region. The porcine stomach size is around 15 cm × 30 cm, with thickness ranging from 50 mm to 60 mm. The porcine intestine region is around 3 cm × 30 cm. All samples are contained in a test box with a width of 18 cm and a length of 40 cm. The flexible endoscope is introduced into the test box via an opening. During the inspection, the instruments can be well tracked, and all the details of the experimental samples can be captured by the 6-DOF flexible endoscope.

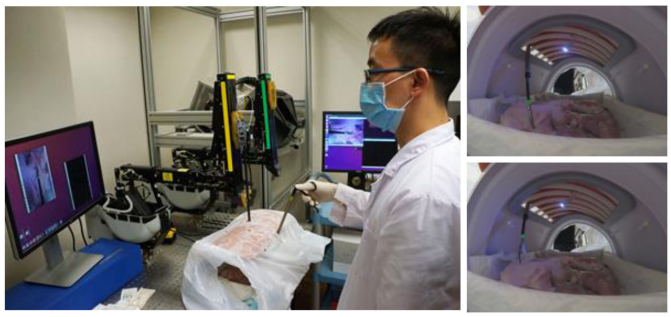

Fig. 10. Intestine and stomach inspection using the proposed endoscope. The left image is the picture of the ex vivo experiment field. And the right images are the images in the model of human body.

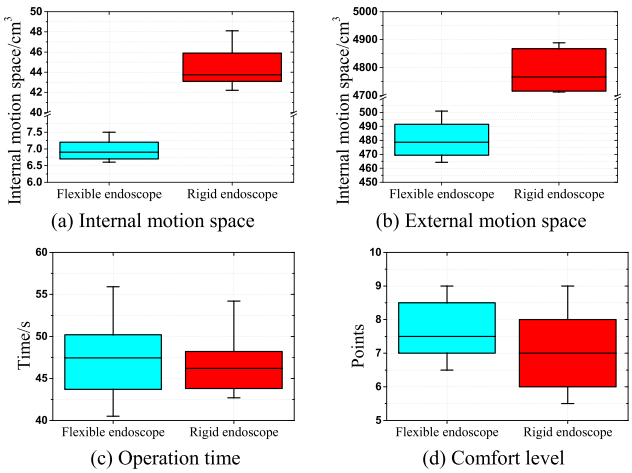

Fig. 11. The comparation between the proposed flexible endoscope and the 4-DOF rigid endoscope. The blue columns are the information for flexible endoscope, and the red columns are the information for the rigid endoscope. (a) occupied space inside of the body during peg transfer task of 10 participants. (b) occupied space outside of the body during peg transfer task of 10 participants. (c) Operation time of the peg transfer time. (d) The scores of the comfort level.

E. User Study

In the fundamentals of laparoscopic surgery (FLS) manual skills, there are 5 training tasks [26]. These tasks include peg transfer, precision cutting, ligating loop, intracorporeal knotting and extracoporeal knotting. During peg transfer, precision cutting and extracorporeal knotting tasks, instruments need to be operated in a relatively large field, which requires manipulating the endoscope to guide the task. Therefore, in the evaluation, three tasks (peg transfer, precision cutting and extracor-

TABLE II
COMPARISON BETWEEN THE FLEXIBLE AND THE RIGID ENDOSCOPE

	4-DOF Rigid endoscope	6-DOF Flexible endoscope
Safety	average level	good
Viewing field	relatively small	relatively large
Motion space	large	small
Operating time	average level	average level
Comfort level	average level	average level

poreal knotting) are chosen to evaluate the performance of the automatic flexible endoscope. The tasks are operated by two hand-held flexible instruments. During the three tasks, the two instruments can be well tracked. What's more, 10 participants (including six participants with engineering background, three medical students and one surgeon) have been invited to do the three FLS tasks using both the flexible endoscope and the 4-DOF rigid endoscope. Then they score for the comfort level of the two endoscopes (0–10 points). The results are shown in Fig. 11.

From Fig. 11, we can see that compared with 4-DOF rigid endoscope, both the internal and external occupied space of the proposed flexible endoscope is significantly reduced, which can enhance the safety of the endoscope system during surgery and enlarge the operating space for surgeons. The scores of the comfort level and the task operation time by using the two endoscopes are very close to each other. The advantages of the proposed flexible endoscope are shown in Table II.

VI. CONCLUSION

In this paper, an automatic 6-DOF flexible endoscope with enhanced safety is presented. The proposed flexible endoscope has a distal bending section based on the TCM. It is integrated with the da Vinci Research Kit (DVRK) with a total of six DOFs. Automatic instruments tracking by visual servoing is achieved. The endoscope movement is minimized by using optimal control method during instrument tracking process. This helps to reduce the instruments fencing inside the surgical cavity as well as arms collision outside the body. Experimental testing are used to evaluate the performance of the proposed automatic flexible endoscope. Experimental results show that the proposed flexible endoscope can well track both stationary and moving targets. In tracking a volume of 200 mm $\times$ 200 mm $\times$ 100 mm, the internal space and external space occupied by the flexible endoscope are 15.55% and 9.87% of conventional rigid endoscopes respectively. This shows that the proposed flexible endoscope could significantly save the space and reduce the safety problems during the MIS procedures. Lastly, user study involving10 subjects validated that the flexible endoscope can be used in MIS tasks and could provide wider field of view, and safer operation compared with rigid endoscopes. Limitations still exist in current system, including blurred image and uneven illumination inside body cavity. Our future work aims at reducing image blur caused by fast motion of instruments. Furthermore, stereoscopic 3D vision will be combined with the proposed system in future development.

REFERENCES

[1] S. Horgan and D. Vanuno, "Robots in laparoscopic surgery," *J. Laparoendoscopic Adv. Surg. Techn.*, vol. 11, no. 6, pp. 415–419, 2001.

[2] M. Hashizume, K. Konishi, K. Okazaki, and K. Tanoue, "Fundamental training for safe endoscopic surgery," *Innov. Med. Technol.*, vol. 49, pp. 49–51, 2005.

[3] J. H. Kaouk *et al.*, "Single-port laparoscopic surgery in urology: initial experience," *Urology*, vol. 71, no. 1, pp. 3–6, 2008.

[4] Z. Li, J. Feiling, H. Ren, and H. Yu, "A novel tele-operated flexible robot targeted for minimally invasive robotic surgery," *Engineering*, vol. 1, no. 1, pp. 73–78, 2015.

[5] T. Yasunaga *et al.*, "Remote-controlled laparoscope manipulator system, naviot, for endoscopic surgery," *Int. Congr. Ser.*, vol. 1256, pp. 678–683, 2003.

[6] Y. Wang, K. P. Laby, D. R. Uecker, A. A. Mangaser, and M. Ghodoussi, "Automated endoscope system for optimal positioning," U.S. Patent 5 878 193, Mar. 2, 1999.

[7] A. Meyer and D. Oleynikov, "Surgical robotics," in *Mastery of Endoscopic and Laparoscopic Surgery,* 4th ed. Norwell, MA, USA: Kluwer, 2013.

[8] M. Kim, C. Lee, N. Hong, Y. J. Kim, and S. Kim, "Development of stereo endoscope system with its innovative master interface for continuous surgical operation," *Biomed. Eng.*, vol. 16, no. 1, pp. 12938–12, 2017.

[9] A. Nishikawa *et al.*, "Face mouse: A novel human-machine interface for controlling the position of a laparoscope," *IEEE Trans. Robot. Automat.*, vol. 19, no. 5, pp. 825–841, Oct. 2003.

[10] C.-A. O. Nathan, V. Chakradeo, K. Malhotra, H. D'Agostino, and R. Patwardhan, "The voice-controlled robotic assist scope holder aesop for the endoscopic approach to the sella," *Skull Base*, vol. 16, no. 3, pp. 123–131, 2006.

[11] U. Schwarz and T. Schmuckle, "Cognitive eyes," *Archives suisses de neurologie et de psychiatrie*, vol. 153, no. 4, pp. 175–179, 2002.

[12] A. C. Schütz, D. I. Braun, and K. R. Gegenfurtner, "Eye movements and perception: A selective review," *J. Vis.*, vol. 11, no. 5, p. 9, 2011.

[13] D. P. Noonan, G. P. Mylonas, J. Shang, C. J. Payne, A. Darzi, and G.-Z. Yang, "Gaze contingent control for an articulated mechatronic laparoscope," in *Proc. 3rd IEEE RAS EMBS Int. Conf. Biomed. Robot. Biomechatronics*, Tokyo, Japan, Sep. 26–29, 2010, pp. 759–764.

[14] K. Fujii, A. Salerno, K. Sriskandarajah, K.-W. Kwok, K. Shetty, and G.-Z. Yang, "Gaze contingent cartesian control of a robotic arm for laparoscopic surgery," in *Proc. IEEE/RSJ Int. Conf. Intell. Robot Syst.*, Tokyo, Japan, Nov. 3–7, 2013, pp. 3582–3589.

[15] A. Agustinos, R. Wolf, J.-A. Long, P. Cinquin, and S. Voros, "Visual servoing of a robotic endoscope holder based on surgical instrument tracking," in *Proc. Biomed. Robot. Biomechatronics*, Sao Paulo, Brazil, Aug. 12–15, 2014, pp. 13–18.

[16] P. Kazanzides, Z. Chen, A. Deguet, G. S. Fis-cher, R. H. Taylor, and S. P. DiMaio, "An open-source research kit for the da vinci® surgical system," in *Proc. IEEE Int. Conf. Robot. Automat.*, HongKong, China, May 31–Jun. 7, 2014, pp. 6434–6439.

[17] Z. Li, M. Z. Oo, V. Nalam, V. D. Thang, H. Ren, T. Ko dis, and H. Yu, "Design of a novel flexible endoscope-cardioscope," *J. Mechanisms Robot.*, vol. 8, no. 5, 2016, Art. no. 051014.

[18] Z. Li, L. Wu, H. Ren, and H. Yu, "Kinematic comparison of surgical tendon-driven manipulators and concentric tube manipulators," *Mechanism Mach. Theory*, vol. 107, pp. 148–165, 2017.

[19] Z. Jia, X. Ma, W. Liu, W. Lu, X. Li, L. Chen, Z. Wang, and X. Cui, "Pose measurement method and experiments for high-speed rolling targets in a wind tunnel," *Sensors*, vol. 14, no. 12, pp. 23 933–23 953, 2014.

[20] Z. Zhang, "Camera calibration with one-dimensional objects," *IEEE Trans. Pattern Anal. Mach. Intell.*, vol. 26, no. 7, pp. 892–899, Jul. 2004.

[21] F. Garcia-Lamont, J. Cervantes, A. Lopez, and L. Rodriguez, "Segmentation of images by color features: A survey," *Neurocomputing*, vol. 292, pp. 1–27, 2018.

[22] J. Weng, P. Cohen, and M. Herniou, "Camera calibration with distortion models and accuracy evaluation," *IEEE Trans. Pattern Anal. Mach. Intell.*, no. 10, pp. 965–980, Oct. 1992.

[23] S. Hutchinson, G. D. Hager, and P. I. Corke, "A tutorial on visual servo control," *IEEE Trans. Robot. Automat.*, vol. 12, no. 5, pp. 651–670, Oct. 1996.

[24] P. I. Corke *et al.*, "High-performance visual servoing," in *Visual Control of Robots*. Taunton, U.K.: Res. Studies Press, 1996.

[25] Y. Chen *et al.*, "Safety-enhanced motion planning for fexible surgical manipulator using neural dynamics," *IEEE Trans. Control Syst. Technol.*, vol. 25, no. 5, pp. 1711–1723, Sep. 2017.

[26] G. M. Fried, "Fls assessment of competency using simulated laparoscopic tasks," *J. Gastrointestinal Surg.*, vol. 12, no. 2, pp. 210–212, 2008.